Vortex and Surface Phase Transitions in Superconducting Higher-order Topological Insulators

Sayed Ali Akbar Ghorashi,[1] Taylor L. Hughes,[2] and Enrico Rossi[1]
[1]*Department of Physics, William & Mary, Williamsburg, Virginia 23187, USA*
[2]*Department of Physics and Institute for Condensed Matter Theory, University of Illinois at Urbana-Champaign, Champaign, Illinois 61801, USA*

(Received 18 October 2019; accepted 30 June 2020; published 17 July 2020)

Topological insulators, having intrinsic or proximity-coupled s-wave superconductivity, host Majorana zero modes (MZMs) at the ends of vortex lines. The MZMs survive up to a critical doping of the TI at which there is a vortex phase transition that eliminates the MZMs. In this work, we show that the phenomenology in higher-order topological insulators (HOTIs) can be qualitatively distinct. In particular, we find two distinct features. (i) We find that vortices placed on the gapped (side) surfaces of the HOTI, exhibit a pair of phase transitions as a function of doping. The first transition is a surface phase transition after which MZMs appear. The second transition is the well-known vortex phase transition. We find that the surface transition appears because of the competition between the superconducting gap and the local $\mathcal{T}$-breaking gap on the surface. (ii) We present numerical evidence that shows strong variation of the critical doping for the vortex phase transition as the center of the vortex is moved toward or away from the hinges of the sample. We believe our work provides new phenomenology that can help identify HOTIs, as well as illustrating a promising platform for the realization of MZMs.

DOI: 10.1103/PhysRevLett.125.037001

Introduction.—In the past decade there has been an explosion of interest in new forms of topological matter, driven by the discoveries of topological insulators and gapless topological semimetals [1–3]. The search for Majorana zero modes (MZMs) has been at the heart of it, due to its promising applications in developing the building blocks of topological quantum computation [4]. In a seminal work, Fu and Kane [5] showed that a MZM can be trapped in the core of a vortex when an s-wave superconductor proximitizes a topological insulator (TI) with gapless, Dirac surface states. Later, Hosur *et al.* [6] demonstrated that these MZMs can actually survive up to some critical doping of the TI bulk bands beyond the band edges [7–9].

Recently, some aspects of topological phases of matter have received newborn attention after the introduction of so-called higher-order topological phases [10–15], which has spawned numerous works in the last few years [16–32]. An nth-order topological phase of a system of dimension d possesses gapless boundary modes on the $d-n$ dimensional boundaries with $1 < n \leq d$, unlike a conventional topological phase for which $n = 1$. Since its first theoretical discovery [10], there have been experimental realizations of higher-order topological insulators (HOTIs) in several metamaterial contexts [33–36], as well as evidence in solid state electronic materials [12].

In light of this previous work we can ask a natural question: can proximitized (or intrinsically superconducting) 3D HOTIs exhibit MZMs in their vortices? In this Letter we answer this question in the affirmative, but we reveal the appearance of a surface phase transition tuned by changes in the chemical potential that distinguishes the HOTI from the ordinary TI phenomenology. We identify the general condition for the appearance of the surface transition making our results relevant to a large class of higher-order 3D topological systems. Recent works [28,37–46] have pointed out that some of the magnetic and axion insulators as well as iron-based superconductors might be related to higher-order topological phases. Also, many experiments [47–51] have studied the physics of vortices in iron-based superconductors. Therefore, these developments suggest that our results might apply to systems that are already actively studied experimentally.

We begin with a conventional 3D $\mathcal{T}$-invariant topological insulator. From here, Ref. [13] predicts that one can form a 3D HOTI having chiral hinge states if one adds a $C_4^z\mathcal{T}$ symmetric term. This term acts to gap out the surfaces perpendicular to the x and y directions, but it leaves the z surfaces gapless. When proximitized by s-wave superconductivity, the z surfaces behave as in an ordinary TI, as long as any vortices are far from any (gapless) hinges of the sample. However, vortices on the side surfaces show a different phenomenology. Besides the large critical doping $\mu^{c,2}$ that marks the known vortex phase transition (VPT) [6], we find a new lower critical doping $\mu^{c,1}$ (Fig. 1). For chemical potentials smaller than $\mu^{c,1}$ no stable MZMs are bound to vortices on the side surfaces. The lower critical

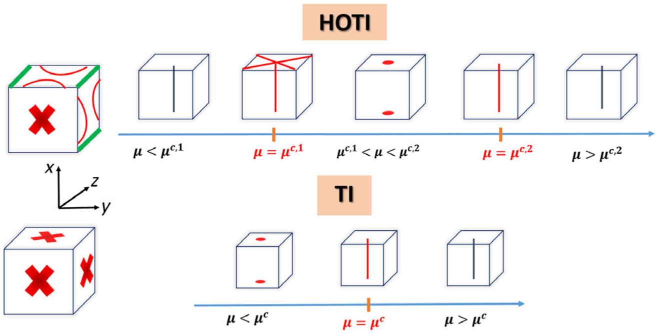

FIG. 1. A schematic picture depicting the evolution of the vortex bound states with doping. The low-energy 1D vortex spectrum can be utilized to distinguish between HOTI (with chiral hinge states) from a conventional TI. By tuning of doping at the critical doping $\mu^{c,1}$, the gapped surfaces of HOTIs undergo a surface phase transition and stable MZMs only appear for $\mu^{c,1} < \mu < \mu^{c,2}$.

point represents a topological surface phase transition resulted from the competition between superconducting gap and the $C_4\mathcal{T}$ symmetric term. Therefore, we find that stable, vortex-bound MZMs do exist on the side surfaces for the range $\mu^{c,1} < \mu < \mu^{c,2}$ (Fig. 1).

We illustrate these transitions, in comparison with an ordinary proximitized TI, in Fig. 1. We believe that our results clearly distinguish the vortex phenomenology in proximity induced TIs and HOTIs, and can be employed as a promising approach for identifying HOTIs as well as platform for the realization of MZMs.

Model.—We begin with a lattice model for a 3D superconducting chiral HOTI with s-wave singlet pairing. Let $\Psi_{\mathbf{k}}^T = (\psi_{\mathbf{k}}, \psi_{-\mathbf{k}}^\dagger)$ where $\psi_{\mathbf{k}}^T = (c_\uparrow, c_\downarrow d_\uparrow, d_\downarrow)$ and (c, d) represent different orbitals while $\uparrow$ and $\downarrow$ are spin. The Bogoliubov–de Gennes (BdG) Hamiltonian for our model is $H_{SC} = \sum_{\mathbf{k}} \Psi_{\mathbf{k}}^\dagger h_{\mathbf{k}}^{\text{BdG}} \Psi_{\mathbf{k}}$ where

$$h_{\mathbf{k}}^{\text{BdG}} = \begin{bmatrix} H_{\text{HOTI}}(\mathbf{k}) - \mu & \Delta \\ \Delta^* & -H_{\text{HOTI}}^T(-\mathbf{k}) + \mu \end{bmatrix} \quad (1)$$

and

$$H_{\text{HOTI}}(\mathbf{k}) = \left(M + t_0 \sum_i \cos(k_i)\right)\kappa_z\sigma_0 + t_1 \sum_i \sin(k_i)\kappa_x\sigma_i + t_2[\cos(k_x) - \cos(k_y)]\kappa_y\sigma_0. \quad (2)$$

κ and σ are Pauli matrices in orbital and spin spaces, respectively, and we set lattice constant to one. For $t_2 = 0$, Eq. (2), represents the well-known model of 3D time-reversal invariant TI, for $1 < |M| < 3$ (strong TI) and $0 < |M| < 1$ (weak TI). For $t_2 \neq 0$ the system can be in a 3D chiral HOTI phase when the TI is tuned to a strong TI phase [13]. The term proportional to t_2 breaks time reversal and C_4 rotational symmetry while preserving their product: $(C_4\mathcal{T})H_{\text{HOTI}}^*(k_x, k_y, k_z)(C_4\mathcal{T})^{-1} = H_{\text{HOTI}}(k_y, -k_x, -k_z)$, $C_4 = \kappa_0 e^{-i\pi\sigma_z/4}$ and $\mathcal{T} = \kappa_0\sigma_y$. As a result, x, y surfaces are gapped while the z surface remains gapless. The model of Eq. (2) is ideal to understand the differences between the vortex phase transition in a superconducting TI and a superconducting HOTI given that (i) it is a prototypical model of chiral HOTI that reduces to a standard TI for $t_2 \to 0$, and (ii) it has two gapless surfaces and therefore allows us to understand how the vortex' spectrum is affected by the nature, gapless or not, of the surfaces of the HOTI, and to understand the differences, for the vortex spectrum, between the gapless surfaces of the TI and the gapless surfaces of the HOTI. We also considered other *standard* HOTI models [14,19,52–55], see the Supplemental Material [56], and found qualitative similar results. For the pairing term (assumed to be s wave) we choose $\Delta = \delta_0\kappa_0\sigma_y$ where δ_0 is the strength of the pairing. We choose this pairing for two reasons: (i) among all the possible s-wave pairing, [56–59], it is the only one for which the bulk remains gapped as the chemical potential is varied, (ii) it is the pairing that was considered in the study of the vortex phase transition in a superconducting TI [6].

In the presence of superconductivity, the HOTI will develop chiral Majorana hinge modes, with a pair of chiral modes on hinges parallel to z that split when they intersect the top and bottom surfaces [60]. We can implement a vortex line in a plane using a spatially dependent pairing term $\Delta(\mathbf{r}) = \Delta \tanh(r/\xi_0)e^{i\phi_0}$, where $r = \sqrt{x_i^2 + x_j^2}$, $\phi_0 = \arctan(x_j/x_i)$, and we choose $\xi_0 = 1$. We ignore any contributions from the vector potential and Zeeman term from the field used to induce the vortex as in Ref. [6]. The model for the strong TI has cubic symmetry so inserting a vortex on surfaces normal to x, y, or z gives rise to the same physics. However, this is not the case for HOTIs, as cubic symmetry is broken to an axial symmetry that distinguishes z from x and y. From the $C_4\mathcal{T}$ symmetry one expects similar behavior for vortices along x and y (up to a time-reversal transformation), but the z direction can be distinct.

Results.—We obtain the low-energy spectrum in the presence of a vortex by numerically diagonalizing the BdG Hamiltonian in Eq. (1) with periodic boundary conditions in the direction parallel to the vortex line (results are shown in Fig. 2). For easy comparison with earlier results [6] we choose the following set of parameters: $M = -2.5$, $t_0 = t_1 = 1$ (in the remainder all energies are in units of t_0). For this choice of parameters all of the interesting physics is happening near the Γ point so we focus on $k_z = 0$ ($k_x = 0$) for vortex lines parallel to z (x).

For the parameters mentioned above, Ref. [6] showed MZMs at the ends of vortex lines survive up to a critical doping of $\mu^c \sim 0.9$ where the vortex lines undergo a VPT. In Fig. 2(a), we have reproduced this result for comparison. For chemical potentials smaller than μ^c the spectrum on the

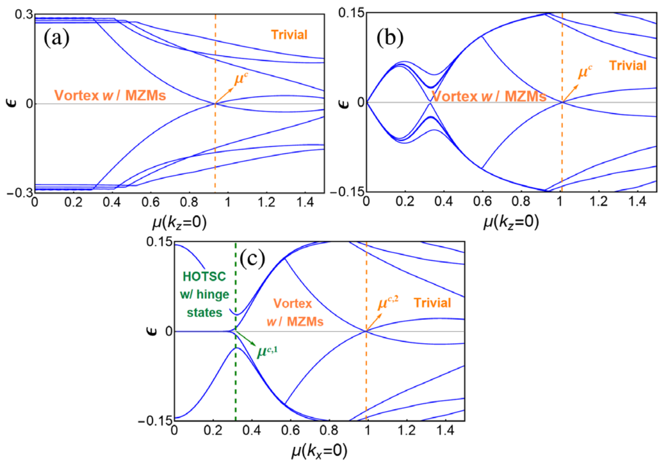

FIG. 2. VPT spectrum versus μ for (a) a TI with vortex line parallel to z, (b) a HOTI with a vortex line parallel to z, (c) a HOTI with a vortex line parallel to x. For (a),(b) the system size is 40×40 in the plane perpendicular to the vortex line. In (c) the system size is 100×100. Model parameters $M = -2.5$, $t_0 = 1$, $t_1 = 1$, $t_2 = 1$, $\delta_0 = 0.3$ are used.

(periodic) vortex line is gapped, and MZMs will appear if the vortex line is terminated at a surface. From symmetry this result is independent of the orientation of the vortex line, e.g., vortex lines parallel to x or z have the same μ^c.

Next, we turn on t_2 to push the system into the HOTI phase and obtain the spectrum for vortex lines oriented in the z [Fig. 2(b)] and the x [Fig. 2(c)] directions. We find that a critical μ still exists around $\mu \sim 1.0$, for both vortex orientations, having only a small increase compared to the TI case. However, we see a qualitative difference for small chemical potentials, i.e., there are other gapless points in Figs. 2(b) and 2(c) that are absent in the case of an ordinary TI. Without a vortex, a HOTI with superconducting pairing, as in Eq. (1), is gapped on all surfaces. However, it possesses low-energy Majorana hinge states for a specific range of μ. In Fig. 2(b) the gapless point at $k_z = 0$ and $\mu = 0$ is the hinge modes of the proximitized HOTI. As μ is tuned away from zero the hinge states parallel to z have their zero-energy nodal point shifted off $k_z = 0$ so we only see finite-energy states associated to the hinges for $\mu \neq 0$. These hinge modes exist up to around $\mu \sim 0.3$ where there is a surface phase transition (see Fig. S1 in the Supplemental Material [56]).

Lets now consider a vortex line parallel to x the corresponding spectrum for $k_x = 0$ is shown in Fig. 2(c). Up to $\mu^{c,1}$ (denoted by green vertical dashed line), there are hinge modes, and for this orientation the zero-energy nodal point is not shifted away from $k_x = 0$ as μ is increased. At $\mu^{c,1}$ there is a surface phase transition, after which the hinge states are removed. For $\mu^{c,1} < \mu < \mu^{c,2}$ the 3D superconducting HOTI is not topological and the only zero energy states are the Majoranas at the ends of the vortex. We show the evolution of the low-energy surface states (without a vortex) in Figs. 3(a)–3(c) as we tune μ through $\mu^{c,1}$. In Figs. 3(e)–3(h) we show the 3D probability densities of low-energy modes when a vortex is present and is oriented along the x direction. We first see hinge states [3(e)] followed by states extended along the surface [3(f)] at the surface phase transition. After the surface phase transition the MZMs appear [3(g)], which are subsequently

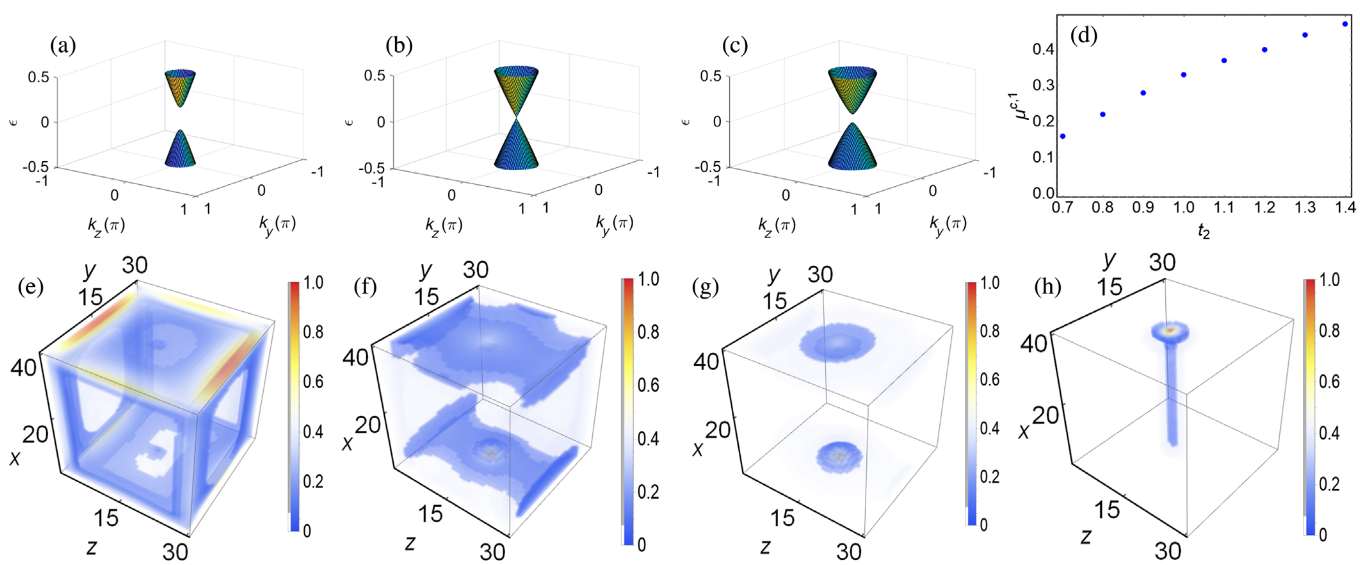

FIG. 3. Surface phase transition in a superconducting HOTI. (a)–(c) The evolution of surface states in the $y - z$ plane for $\mu = 0.1$, 0.33, 0.4, respectively. A surface phase transition occurs at $\mu^{c,1} \sim 0.33$. (d) $\mu^{c,1}$ versus t_2. (e)–(h) The evolution of the probability density profile of the lowest energy states when a vortex is inserted perpendicular to the $y - z$ surface and μ is tuned. (e) Hinge modes, (f) surface phase transition at $\mu^{c,1}$, (g) Majorana zero modes, (h) vortex phase transition at $\mu^{c,2}$. $M = -2.5$, $t_1 = 1$, $t_2 = 1$, $\delta_0 = 0.3$. Lattices of size of $40 \times 30 \times 30$ are used to obtain the 3D probability density profiles.

destroyed at $\mu^{c,2}$ [3(h)]. Remarkably, we see that the MZMs appear only after the surface phase transition. This is in sharp contrast to the surfaces of the TI and the (001) surface of the HOTI as these always host MZMs as long as $\mu < \mu^{c,2}$.

To get a clearer understanding of the surface phase transition demonstrated in Fig. 3, we derive an effective surface Hamiltonian for the (100) surface of the superconducting HOTI by treating the $C_4^z\mathcal{T}$ symmetric term in Eq. (2) perturbatively. We find $h_{\rm eff}(\mathbf{k}) = v_z k_z \tau_z \sigma_y + v_y k_y \tau_0 \sigma_z - (t_2/2)\tau_z\sigma_x + \delta_0 \tau_y \sigma_y - \mu \tau_z \sigma_0$. We see that both the $C_4\mathcal{T}$ symmetric term, and the superconducting pairing, can independently gap out the surface states (since they both fully anticommute with the kinetic energy terms), but they commute with each other, therefore they can be thought of as *competing* masses on the surface. This can lead to a gap closure at $k_y = k_z = 0$ when $\mu^c = \sqrt{t_2^2 - 4\delta_0^2}/2$. This is a general condition, therefore we expect that a surface transition will occur in any other model of chiral HOTIs for which the surface projection of the mass and superconducting pairing term commute. Similarly, for 3D HOTIs constructed by gluing together lower-dimensional topological phases [19,61,62] to have a surface phase transition the mass terms of the 2D surfaces connected by the vortex must commute with the superconducting pairing term. A prediction from this analysis is that a surface phase transition only appears in the $t_2 > 2\delta_0$ regime, i.e., when the local $\mathcal{T}$-breaking surface gap is stronger than the proximity-induced gap. To show this more rigorously we compute $\mu^{c,1}$ numerically by varying t_2 for a fixed δ_0. From Fig. 3(d), we clearly see that, for a fixed superconducting gap δ_0, when increasing t_2, $\mu^{c,1}$ increases in qualitative agreement with the analytical result.

We now show that, in addition to the chemical potential, an external Zeeman term can provide some amount of tunability of the surface phase transition. Let us consider a vortex line along the x direction passing through the center of the $y-z$ plane. An external magnetic field B_x in the x direction gives rise to the Zeeman term $B_x J_x = B_x \tau_z \kappa_0 \sigma_x$. This term can partially suppress the effect of t_2. $B_x = 0.1$, for example, reduces $\mu^{c,1}$ from 0.33 to 0.16. For sufficiently strong magnetic field, the phase appears after the surface phase transition can still possess Majorana hinge states [63]. A Zeeman field perpendicular to the vortex line (i.e., parallel to the surface) will not influence $\mu^{c,1}$. Therefore, we find that we can tune the surface phase transition on a given surface by applying a Zeeman field. If one has control over the orientation of the field one may be able to selectively tune the critical doping levels on each surface.

Now, we briefly discuss how the location of the vortex center (V_c) on the side surfaces affects the critical doping $\mu^{c,2}$. Let the distance between the vortex center and the hinge at corner (1,1) be $d_h = (n-1)\sqrt{2}$, and the distance between the vortex center and the center of the plane be $d_c = (N/2 - n)\sqrt{2}$, where the surface is an $N \times N$ square, and n is the coordinate of the vortex center along the diagonal [Fig. 4(a)]. Figure 4(b) shows $\mu^{c,2}$ versus d_h, for two different system sizes, $N = 24$, 28. By changing, the system size, d_c changes but d_h remains same. By decreasing d_h we find (unlike the TIs or HOTIs with a vortex parallel to the z direction) $\mu^{c,2}$ increases and the results are independent of N, therefore we conclude that this is not a finite-size effect and that the vortex is sensitive to d_h. The details of the variation (and how strong the variation is), are a function of various parameters of the system, and in some cases can be affected more strongly by finite size effects. We note that for a fixed set of system parameters, the variation of d_h only affects $\mu^{c,2}$ and not $\mu^{c,1}$ as the surface physics is nominally insensitive to the presence of the vortex. However, an external Zeeman term could affect the results of Fig. 4(b) indirectly, since the presence or absence or spatial profile of the hinge states are effected by the Zeeman field, and thus the vortex-hinge hybridization can be affected by such a field. This effect may be difficult to observe with a single (likely pinned) vortex, but may be measureable with a vortex lattice where one might expect a distribution of $\mu^{c,2}$ across the lattice depending on the spatial location of the vortices relative to the hinges.

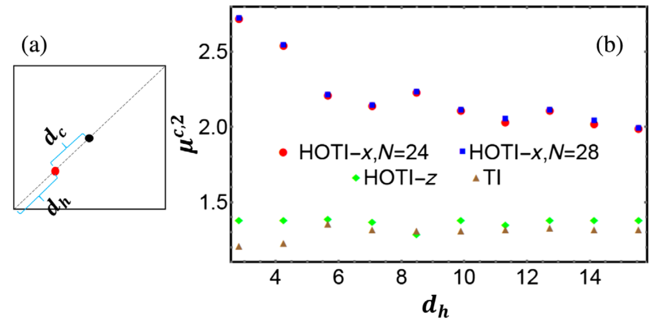

FIG. 4. (a) schematic picture shows the distance between a vortex (red dot) from hinge d_h and center d_c of lattice (black dot), (b) $\mu^{c,2}$ versus d_h for HOTI with superconducting vortex along the x direction (HOTI x) with two system sizes of $N = 24$, 28 and HOTI z and TI with $N = 28$. $M = -2$, $t_1 = 1$, $t_2 = 1$(HOTI), $\delta_0 = 0.2$.

In summary, we have found that vortex phenomenology can be utilized to distinguish a class of HOTIs from TIs, and can also serve as a platform for the realization of Majorana zero modes. In HOTIs having proximity-induced or intrinsic s-wave superconductivity we identified a new critical doping $\mu^{c,1}$ that marks a topological surface phase transition for the gapped surfaces. We showed that MZMs only appear in a range of doping levels between $\mu^{c,1}$ and $\mu^{c,2}$, the latter being the critical doping for the known vortex phase transition. The surface transition results from two competing mass terms on the gapped surfaces of HOTI: the superconducting gap and a $\mathcal{T}$-breaking mass term resulting from the bulk $C_4\mathcal{T}$ symmetric term that is responsible for driving a parent $\mathcal{T}$-invariant TI into the HOTI. We note that the latter condition is general and surface phase transition should occur in any chiral HOTIs for which the projection on the surfaces connected by the vortex of the mass term and of the superconducting pairing term commute. In the Supplemental Material [56], we consider two other HOTI models to exemplify this general condition.

The surface phase transition can be tuned with chemical potential or Zeeman fields which may help the experimental detection of the phase transitions and MZMs. Recently, iron-based superconductors attracted attention because they can host both topological and trivial vortices simultaneously [47–51,64–68]. Here we have shown that the HOTIs are another example of such systems, which, for a specific range of dopings and applied Zeeman fields, can host both trivial and topological vortices, but in different orientations. We have provided numerical evidence showing strong variation of the critical doping $\mu^{c,2}$ depending on the spatial location of the vortex center. Very recently, several materials and heterostructures have been proposed as possible chiral HOTIs: $EuIn_2As_2$ [37], $EuSn_2As_2$ [43], $MnBi2Te_4$ [39–43], and $CrI_3/Bi_2Se_3/MnBi_2Se_4$ heterostructures [38]. A possible setup to observe our theoretical predictions could be realized by combining one of the materials above in a heterostructure consisting of an s-wave superconductor and an external gate (separated by the HOTI by a high quality dielectric) to tune the chemical potential of the HOTI, in which a vortex is induced via an external magnetic field along the x direction (see also the Supplemental Material [56]).

S. A. A. G. and E. R. acknowledge support from ARO (Grant No. W911NF-18-1-0290), NSF (Grant No. DMR-1455233). E. R. also thanks the Aspen Center for Physics, which is supported by NSF Grant No. PHY-1607611, where part of this work was performed. The authors acknowledge William & Mary Research Computing for providing computational resources that have contributed to the results reported within this Letter. T. L. H. thanks the U.S. National Science Foundation under Grant No. DMR 1351895-CAR, and the MRSEC program under NSF Grant No. DMR-1720633 (SuperSEED) for support. T. L. H. and E. R. also thank the National Science Foundation under Grant No. NSF PHY1748958(KITP) for partial support at the end stage of this work during the Topological Quantum Matter program and Spin and Heat Transport in Quantum and Topological Materials, respectively.

[1] M. Z. Hasan and C. L. Kane, Colloquium: Topological insulators, Rev. Mod. Phys. **82**, 3045 (2010).
[2] X.-L. Qi and S.-C. Zhang, Topological insulators and superconductors, Rev. Mod. Phys. **83**, 1057 (2011).
[3] C.-K. Chiu, J. C. Y. Teo, A. P. Schnyder, and S. Ryu, Classification of topological quantum matter with symmetries, Rev. Mod. Phys. **88**, 035005 (2016).
[4] C. Nayak, S. H. Simon, A. Stern, M. Freedman, and S. Das Sarma, Non-abelian anyons and topological quantum computation, Rev. Mod. Phys. **80**, 1083 (2008).
[5] L. Fu and C. L. Kane, Superconducting Proximity Effect and Majorana Fermions at the Surface of a Topological Insulator, Phys. Rev. Lett. **100**, 096407 (2008).
[6] P. Hosur, P. Ghaemi, R. S. K. Mong, and A. Vishwanath, Majorana Modes at the Ends of Superconductor Vortices in Doped Topological Insulators, Phys. Rev. Lett. **107**, 097001 (2011).
[7] C.-K. Chiu, M. J. Gilbert, and T. L. Hughes, Vortex lines in topological insulator-superconductor heterostructures, Phys. Rev. B **84**, 144507 (2011).
[8] H.-H. Hung, P. Ghaemi, T. L. Hughes, and M. J. Gilbert, Vortex lattices in the superconducting phases of doped topological insulators and heterostructures, Phys. Rev. B **87**, 035401 (2013).
[9] H.-H. Sun and J.-F. Jia, Detection of majorana zero mode in the vortex, npj Quantum Mater. **2**, 34 (2017).
[10] W. A. Benalcazar, B. A. Bernevig, and T. L. Hughes, Quantized electric multipole insulators, Science **357**, 61 (2017).
[11] W. A. Benalcazar, B. A. Bernevig, and T. L. Hughes, Selected for a viewpoint in physics electric multipole moments, topological multipole moment pumping, and chiral hinge states in crystalline insulators, Phys. Rev. B **96**, 245115 (2017).
[12] F. Schindler, Z. Wang, M. G. Vergniory, A. M. Cook, A. Murani, S. Sengupta, A. Y. Kasumov, R. Deblock, S. Jeon, I. Drozdov, H. Bouchiat, S. Guéron, A. Yazdani, B. A. Bernevig, and T. Neupert, Higher-order topology in bismuth, Nat. Phys. **14**, 918 (2018).
[13] F. Schindler, A. M. Cook, M. G. Vergniory, Z. Wang, S. S. P. Parkin, B. A. Bernevig, and T. Neupert, Higher-order topological insulators, Sci. Adv. **4**, eaat0346 (2018).
[14] J. Langbehn, Y. Peng, L. Trifunovic, F. von Oppen, and P. W. Brouwer, Reflection-Symmetric Second-Order Topological Insulators and Superconductors, Phys. Rev. Lett. **119**, 246401 (2017).
[15] Z. Song, Z. Fang, and C. Fang, $(d-2)$-Dimensional Edge States of Rotation Symmetry Protected Topological States, Phys. Rev. Lett. **119**, 246402 (2017).
[16] S. A. A. Ghorashi, X. Hu, T. L. Hughes, and E. Rossi, Second-order dirac superconductors and magnetic field induced majorana hinge modes, Phys. Rev. B **100**, 020509(R) (2019).
[17] M. Ezawa, Higher-Order Topological Insulators and Semimetals on the Breathing Kagome and Pyrochlore Lattices, Phys. Rev. Lett. **120**, 026801 (2018).
[18] M. Ezawa, Minimal models for wannier-type higher-order topological insulators and phosphorene, Phys. Rev. B **98**, 045125 (2018).
[19] E. Khalaf, Higher-order topological insulators and superconductors protected by inversion symmetry, Phys. Rev. B **97**, 205136 (2018).
[20] D. Călugăru, V. Juričić, and B. Roy, Higher-order topological phases: A general principle of construction, Phys. Rev. B **99**, 041301(R) (2019).

[21] M. Kheirkhah, Y. Nagai, C. Chen, and F. Marsiglio, Majorana corner flat bands in two-dimensional second-order topological superconductors, Phys. Rev. B **101**, 104502 (2020).
[22] Z. Yan, F. Song, and Z. Wang, Majorana Corner Modes in a High-Temperature Platform, Phys. Rev. Lett. **121**, 096803 (2018).
[23] C.-H. Hsu, P. Stano, J. Klinovaja, and D. Loss, Majorana Kramers Pairs in Higher-Order Topological Insulators, Phys. Rev. Lett. **121**, 196801 (2018).
[24] Y. Wang, M. Lin, and T. L. Hughes, Weak-pairing higher order topological superconductors, Phys. Rev. B **98**, 165144 (2018).
[25] Q. Wang, C.-C. Liu, Y.-M. Lu, and F. Zhang, High-Temperature Majorana Corner States, Phys. Rev. Lett. **121**, 186801 (2018).
[26] T. Liu, J. J. He, and F. Nori, Majorana corner states in a two-dimensional magnetic topological insulator on a high-temperature superconductor, Phys. Rev. B **98**, 245413 (2018).
[27] X. Zhu, Second-Order Topological Superconductors with Mixed Pairing, Phys. Rev. Lett. **122**, 236401 (2019).
[28] R.-X. Zhang, W. S. Cole, and S. Das Sarma, Helical Hinge Majorana Modes in Iron-Based Superconductors, Phys. Rev. Lett. **122**, 187001 (2019).
[29] S. Franca, D. V. Efremov, and I. C. Fulga, Phase-tunable second-order topological superconductor, Phys. Rev. B **100**, 075415 (2019).
[30] Z. Yan, Majorana corner and hinge modes in second-order topological insulator-superconductor heterostructures, Phys. Rev. B **100**, 205406 (2019).
[31] Y.-T. Hsu, W. S. Cole, R.-X. Zhang, and J. D. Sau, Inversion-protected higher order topological superconductivity in monolayer WTe_2, arXiv:1904.06361.
[32] S.-B. Zhang and B. Trauzettel, Detection of second-order topological superconductors by Josephson junctions, Phys. Rev. Research **2**, 012018 (2020).
[33] C. W. Peterson, W. A. Benalcazar, T. L. Hughes, and G. Bahl, A quantized microwave quadrupole insulator with topologically protected corner states, Nature (London) **555**, 346 (2018).
[34] J. Noh, W. A. Benalcazar, S. Huang, M. J. Collins, K. P. Chen, T. L. Hughes, and M. C. Rechtsman, Topological protection of photonic mid-gap defect modes, Nat. Photonics **12**, 408 (2018).
[35] M. Serra-Garcia, V. Peri, R. Süsstrunk, O. R. Bilal, T. Larsen, L. G. Villanueva, and S. D. Huber, Observation of a phononic quadrupole topological insulator, Nature (London) **555**, 342 (2018).
[36] S. Imhof, C. Berger, F. Bayer, J. Brehm, L. W. Molenkamp, T. Kiessling, F. Schindler, C. H. Lee, M. Greiter, T. Neupert, and R. Thomale, Topolectrical-circuit realization of topological corner modes, Nat. Phys. **14**, 925 (2018).
[37] Y. Xu, Z. Song, Z. Wang, H. Weng, and X. Dai, Higher-Order Topology of the Axion Insulator $euin_2as_2$, Phys. Rev. Lett. **122**, 256402 (2019).
[38] Y. S. Hou, J. W. Kim, and R. Q. Wu, Axion insulator state in ferromagnetically ordered $Cri_3/Bi_2Se_3/MnBi_2Se_4$ heterostructures, Phys. Rev. B **101**, 121401(R) (2020).
[39] D. Zhang, M. Shi, T. Zhu, D. Xing, H. Zhang, and J. Wang, Topological Axion States in the Magnetic Insulator $mnbi_2te_4$ with the Quantized Magnetoelectric Effect, Phys. Rev. Lett. **122**, 206401 (2019).
[40] Yan Gong *et al.*, Experimental realization of an intrinsic magnetic topological insulator, Chin. Phys. Lett. **36**, 076801 (2019).
[41] Y.-J. Hao, P. Liu, Y. Feng, X.-M. Ma, E. F. Schwier, M. Arita, S. Kumar, C. Hu, R. Lu, M. Zeng, Y. Wang, Z. Hao, H.-Y. Sun, K. Zhang, J. Mei, N. Ni, L. Wu, K. Shimada, C. Chen, Q. Liu, and C. Liu, Gapless Surface Dirac Cone in Antiferromagnetic Topological Insulator $mnbi_2te_4$, Phys. Rev. X **9**, 041038 (2019).
[42] Y. J. Chen, L. X. Xu, J. H. Li, Y. W. Li, H. Y. Wang, C. F. Zhang, H. Li, Y. Wu, A. J. Liang, C. Chen, S. W. Jung, C. Cacho, Y. H. Mao, S. Liu, M. X. Wang, Y. F. Guo, Y. Xu, Z. K. Liu, L. X. Yang, and Y. L. Chen, Topological Electronic Structure and its Temperature Evolution in Antiferromagnetic Topological Insulator $mnbi_2te_4$, Phys. Rev. X **9**, 041040 (2019).
[43] H. Li *et al.*, Dirac Surface States in Intrinsic Magnetic Topological Insulators $eusn_2as_2$ and $mnbi_{2n}te_{3n+1}$, Phys. Rev. X **9**, 041039 (2019).
[44] Z. Wang, J. O. Rodriguez, L. Jiao, S. Howard, M. Graham, G. Gu, T. L. Hughes, D. K. Morr, and V. Madhavan, Evidence for dispersing 1d majorana channels in an iron-based superconductor, Science **367**, 104 (2020).
[45] M. J. Gray, J. Freudenstein, S. Y. F. Zhao, R. OConnor, S. Jenkins, N. Kumar, M. Hoek, A. Kopec, S. Huh, T. Taniguchi *et al.*, Evidence for helical hinge zero modes in an fe-based superconductor, Nano Lett. **19**, 4890 (2019).
[46] R.-X. Zhang, W. S. Cole, X. Wu, and S. Das Sarma, Higher-Order Topology and Nodal Topological Superconductivity in fe(se,te) Heterostructures, Phys. Rev. Lett. **123**, 167001 (2019).
[47] P. Zhang, K. Yaji, T. Hashimoto, Y. Ota, T. Kondo, K. Okazaki, Z. Wang, J. Wen, G. D. Gu, H. Ding, and S. Shin, Observation of topological superconductivity on the surface of an iron-based superconductor, Science **360**, 182 (2018).
[48] T. Machida, Y. Sun, S. Pyon, S. Takeda, Y. Kohsaka, T. Hanaguri, T. Sasagawa, and T. Tamegai, Zero-energy vortex bound state in the superconducting topological surface state of fe (se, te), Nat. Mater. **18**, 811 (2019).
[49] D. Wang, L. Kong, P. Fan, H. Chen, S. Zhu, W. Liu, L. Cao, Y. Sun, S. Du, J. Schneeloch, R. Zhong, G. Gu, L. Fu, H. Ding, and H.-J. Gao, Evidence for majorana bound states in an iron-based superconductor, Science **362**, 333 (2018).
[50] L. Kong, S. Zhu, M. Papaj, H. Chen, L. Cao, H. Isobe, Y. Xing, W. Liu, D. Wang, P. Fan, Y. Sun, S. Du, J. Schneeloch, R. Zhong, G. Gu, L. Fu, H.-J. Gao, and H. Ding, Half-integer level shift of vortex bound states in an iron-based superconductor, Nat. Phys. **15**, 1181 (2019).
[51] P. Zhang *et al.*, Multiple topological states in iron-based superconductors, Nat. Phys. **15**, 41 (2019).
[52] O. Pozo, C. Repellin, and A. G. Grushin, Quantization in Chiral Higher Order Topological Insulators: Circular Di-

chroism and Local Chern Marker, Phys. Rev. Lett. **123**, 247401 (2019).
[53] M. Sitte, A. Rosch, E. Altman, and L. Fritz, Topological Insulators in Magnetic Fields: Quantum Hall Effect and Edge Channels with a Nonquantized θ Term, Phys. Rev. Lett. **108**, 126807 (2012).
[54] F. Zhang, C. L. Kane, and E. J. Mele, Surface State Magnetization and Chiral Edge States on Topological Insulators, Phys. Rev. Lett. **110**, 046404 (2013).
[55] M. Ezawa, Magnetic second-order topological insulators and semimetals, Phys. Rev. B **97**, 155305 (2018).
[56] See the Supplemental Materials at http://link.aps.org/supplemental/10.1103/PhysRevLett.125.037001 For hinge spectrum of superconducting HOTI, VPT spectrum of two other models of HOTI, the VPT spectrum for 5 other superconducting pairings and a possible experimental setup.
[57] T. Hashimoto, S. Kobayashi, Y. Tanaka, and M. Sato, Superconductivity in doped dirac semimetals, Phys. Rev. B **94**, 014510 (2016).
[58] L. Fu and E. Berg, Odd-Parity Topological Superconductors: Theory and Application to $cu_x bi_2 se_3$, Phys. Rev. Lett. **105**, 097001 (2010).
[59] B. Roy, S. A. A. Ghorashi, M. S. Foster, and A. H. Nevidomskyy, Topological superconductivity of spin-3/2 carriers in a three-dimensional doped luttinger semimetal, Phys. Rev. B **99**, 054505 (2019).
[60] R. Queiroz and A. Stern, Splitting the Hinge Mode of Higher-Order Topological Insulators, Phys. Rev. Lett. **123**, 036802 (2019).
[61] Z. Song, S.-J. Huang, Y. Qi, C. Fang, and M. Hermele, Topological states from topological crystals, Sci. Adv. **5**, eaax2007 (2019).
[62] E. Khalaf, H. C. Po, A. Vishwanath, and H. Watanabe, Symmetry Indicators and Anomalous Surface States of Topological Crystalline Insulators, Phys. Rev. X **8**, 031070 (2018).
[63] S. A. A. Ghorashi (to be published).
[64] K. Jiang, X. Dai, and Z. Wang, Quantum Anomalous Vortex and Majorana Zero Mode in Iron-Based Superconductor fe (te,se), Phys. Rev. X **9**, 011033 (2019).
[65] E. J. König and P. Coleman, Crystalline-Symmetry-Protected Helical Majorana Modes in the Iron Pnictides, Phys. Rev. Lett. **122**, 207001 (2019).
[66] S. Qin, L. Hu, X. Wu, X. Dai, C. Fang, F.-C. Zhang, and J. Hu, Topological vortex phase transitions in iron-based superconductors, Sci. Bull. **64**, 1207 (2019).
[67] A. Ghazaryan, P. L. S. Lopes, P. Hosur, M. J. Gilbert, and P. Ghaemi, Effect of zeeman coupling on the majorana vortex modes in iron-based topological superconductors, Phys. Rev. B **101**, 020504(R) (2020).
[68] G. Xu, B. Lian, P. Tang, X.-L. Qi, and S.-C. Zhang, Topological Superconductivity on the Surface of fe-Based Superconductors, Phys. Rev. Lett. **117**, 047001 (2016).